BESTROPHINOPATHY

A Spectrum of Ocular Abnormalities Caused by the c.614T>C Mutation in the *BEST1* Gene

LISA TOTO, MD, PHD,* CAMIEL J. F. BOON, MD, PHD, FEBOPHTH,† LUCA DI ANTONIO, MD, PHD,*
MAURIZIO BATTAGLIA PARODI, MD,‡ RODOLFO MASTROPASQUA, MD,§
IVANA ANTONUCCI, PHD,¶ LIBORIO STUPPIA, MD,¶ LEONARDO MASTROPASQUA, MD*

Purpose: To describe the variable ocular phenotype associated with a heterozygous mutation in the *BEST1* gene.

Methods: Clinical and genetic assessment was performed in five members of the same family. Molecular genetic analysis of the *BEST1* gene was performed by direct sequencing. Extensive ophthalmic examination included color fundus imaging, spectral domain optical coherence tomography, fundus autofluorescence, electro-oculography (EOG), and full-field electroretinography (ERG). The main outcome measures were *BEST1* mutations, imaging, and electroretinography findings.

Results: All affected family members carried a single heterozygous c.614T>C (p.I205T) mutation in exon 5 of the *BEST1* gene. The 46-year-old proband showed nanophthalmos with chorioretinal atrophy in the macula, extensive coarse hyperpigmentation in the (mid) peripheral retina with tractional vitreous strands. Full-field ERG revealed nonrecordable cone and rod responses, and EOG showed an absent light rise. The daughter and son of the proband showed a phenotype resembling autosomal recessive bestrophinopathy, including short axial lengths, cystoid fluid collections, and shallow serous subretinal fluid accumulation on spectral domain optical coherence tomography throughout the macula in combination with mild retinal pigment epithelium changes. The son of the proband also showed subretinal yellowish deposits inferiorly in the macula as well as outside the temporal vascular arcade, that were hyperfluorescent on fundus autofluorescence, similar to those seen in autosomal recessive bestrophinopathy. Full-field ERG revealed a reduced rod and cone response and a markedly reduced or absent EOG light peak in both brother and sister of the proband.

Conclusion: The clinical spectrum of bestrophinopathy may encompass severe ocular phenotypes that affect the development and function of the entire eye. A clinical picture similar to autosomal recessive bestrophinopathy can also be caused by a single heterozygous mutation in the *BEST1* gene, such as the c.614T>C (p.I205T) variant in this family.

RETINA 36:1586–1595, 2016

Mutations in the *BEST1* gene cause a spectrum of clinical phenotypes known as the bestrophinopathies, with Best vitelliform macular dystrophy (BVMD) being the most common *BEST1*-associated phenotype.[1–3] More than 100 different mutations of *BEST1* have been reported in BVMD.[3]

A variety of other retinal diseases caused by *BEST1* gene mutations have been reported, some with either predominantly macular alterations such adult-onset foveomacular vitelliform dystrophy,[4,5] or phenotypes with more widespread ocular abnormalities, such as autosomal-dominant vitreoretinochoroidopathy,[6,7] autosomal-dominant microcornea, rod-cone dystrophy,[8] early-onset cataract, and posterior staphyloma (MRCS) syndrome, and atypical retinitis pigmentosa.[9] In addition, autosomal recessive bestrophinopathy (ARB) disease is caused by homozygous or compound heterozygous mutations in the *BEST1* gene.[9–14] Retinal abnormalities in ARB are often accompanied by high hyperopia and a shallow anterior chamber.[7]

The *BEST1* gene, previously known as the *VMD2* gene, encodes the bestrophin-1 protein which belongs to the bestrophin family of anion channels. Bestrophin-1 is a transmembrane protein primarily which is

expressed both in the basolateral membrane of the retinal pigment epithelium (RPE), and intracellularly. Bestrophin-1 functions as a Cl^- channel activated by intracellular Ca^{2+}.[3,15,16]

In contrast to the autosomal-dominant bestrophinopathies, the ARB phenotype is hypothesized to result from biallelic null mutations in the *BEST1* gene.[10]

The clinical features of ARB consist of central vision loss, abnormal full-field electroretinography (ERG) indicating panretinal photoreceptor dysfunction (in contrast to BVMD), and a markedly decreased to absent light rise on the electro-oculogram (EOG) which is seen in virtually all bestrophinopathy cases. On fundoscopy, widespread RPE irregularities, vitelliform deposits in the posterior pole that can be more clearly demonstrated on autofluorescence imaging, and presence of intraretinal and subretinal fluid in the macula are observed.[3,11,17] Because of anterior chamber dysgenesis, ARB can be complicated by angle-closure glaucoma.[18]

In this study, we describe the variable clinical spectrum of bestrophinopathy associated with a single heterozygous mutation in the BEST1 gene.

Methods

Three family members were examined at the Retina Service of the Ophthalmology clinic, University "G. D'Annunzio," Chieti, Italy.

Full clinical assessment performed in these family members included: medical history, best-corrected visual acuity, ocular biometry, fundoscopy, color fundus photography, fundus autofluorescence (Spectralis, HRA + OCT; Heidelberg Engineering, Heidelberg, Germany), and spectral domain optical coherence tomography (Spectralis; HRA + OCT, Heidelberg Engineering).

In addition, the electrophysiology assessment was also performed including EOG and full-field ERG (Retimax electrophysiology system; CSO Srl, Firenze, Italy) according to the International Society for Clinical Electrophysiology of Vision (ISCEV) standards. In addition, ophthalmological information was collected from two affected family members who were unable to undergo clinical evaluation in the aforementioned department.

Genetic Analysis

Genomic DNA of five affected family members was extracted from peripheral blood and buccal cells swab using a BioRobot EZ1instrument (Qiagen, Milan, Italy) according to the manufacturer's protocol, at the Molecular Genetics service of the Chieti University. Amplification of all coding exons and of each flanking intron of *BEST1* gene was performed using polymerase chain reaction followed by direct DNA sequencing.

The study adhered to the tenets of the Declaration of Helsinki, and informed consent was obtained from all subjects. Institutional review board approval was received.

Results

Clinical Findings

Three affected family members from one family of European ethnicity were examined. Anamnestic information and previous imaging of the retina of other two family members were collected. The pedigree is shown in Figure 1.

The proband (Patient III: 7), a 46-year-old white woman, was diagnosed by an ophthalmologist with "macular dystrophy" at the age of 17. A family history of retinal problems was reported. No consanguineous marriage in the genealogic tree was described. Her visual acuity was 0.3 logMAR (20/40) in both eyes. A fundus fluorescein angiography performed at the age of 22 showed uneven hyperfluorescence in the posterior pole related to the RPE atrophic changes. We examined this patient at age 46, when her best corrected visual acuity was hand movements (20/ 20.000) in both eyes. Her refraction was S + 6.75 = C + 0.50 @ 90° in the right eye and S + 4.50 = C + 1.50 @10° in the left eye. Biometric assessment with the IOL Master (Carl Zeiss Meditec AG, Jena, Germany) showed an axial length (AXL) of 19.50 mm and an anterior chamber depth (ACD) of 2.78 mm in the right eye, and an AXL of 19.70 mm and an ACD of 2.67 mm in the left eye. Biomicroscopic fundus examination showed attenuation of the retinal arteries in both eyes, atrophic changes of the RPE-choriocapillaris complex in the macula, bordered by focal hyperpigmentation (Figure 2, A and B). Nasally to the optic disc, 2 areas of subretinal yellowish deposits were present in the right eye (Figure 2A). In the midperipheral and peripheral retina, areas

From the *Department of Medicine and Science of Aging, Eye Clinic, University "G. D'Annunzio" Chieti-Pescara, Chieti, Italy; †Department of Ophthalmology, Leiden University Medical Center, Leiden, the Netherlands; ‡Department of Ophthalmology, University Vita-Salute, Scientific Institute San Raffaele, Milano, Italy; §Ophthalmology Section, Department of Medicine Surgery and Neuroscience, University of Siena, Siena, Italy; and ¶Department of Oral Sciences, Nano and Biotechnologies, "G. d'Annunzio" University, Chieti, Italy.

None of the authors have any financial/conflicting interests to disclose.

L. Toto and C. J. F. Boon equally contributed to the article and should be considered as co-first authors.

Reprint requests: Camiel J. F. Boon, MD, PhD, FEBOphth; e-mail: C.J.F.Boon@lumc.nl

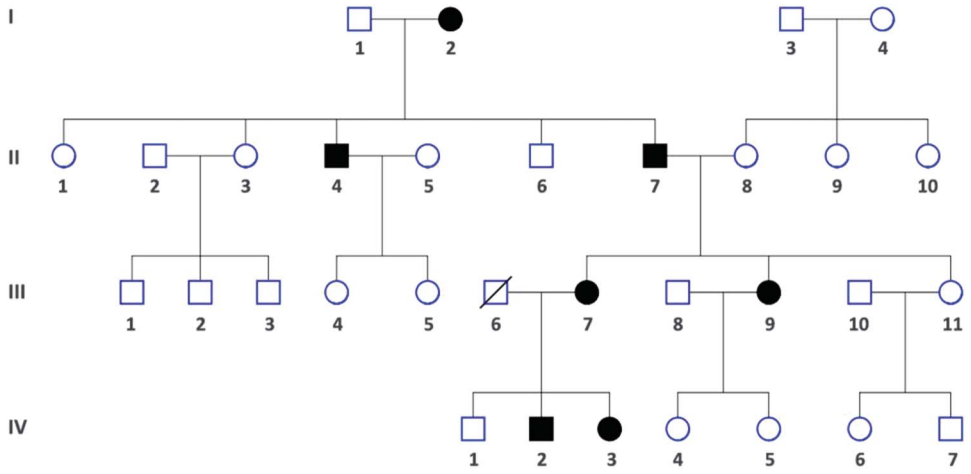

Fig. 1. Pedigree of the family.

of coarse hyperpigmentation and some bone-spicule hyperpigmentation were observed in all quadrants, whereas small dot-shaped yellowish depositions were visible in the inferior, temporal, and nasal midperipheral retina. Throughout the retina from the optic disc to the extreme periphery, midperipheral epiretinal membranes were present in both eyes, and vitreous strands were evident in the right eye (Figure 2, A and B).

Fundus autofluorescence showed patchy hypoautofluorescence in the posterior pole of both eyes, particularly in the macular area, due to RPE atrophy. In the right eye, 2 hyperautofluorescent areas nasally to the optic disc corresponded to the yellowish subretinal deposits on fundoscopy, probably reflecting lipofuscin deposition (Figure 2, C and D). A diffuse oval-shaped zone of hyperautofluorescence was seen in the area of the retinal vascular arcades in both eyes. In the midperipheral and peripheral retina extensive areas of hypoautofluorescence corresponded to confluent atrophic zones with hyperpigmentation on ophthalmoscopy (Figure 2, C and D).

Spectral domain optical coherence tomography images from the horizontal scans centered on the fovea showed an increased reflectivity of the vitreoretinal interface in both eyes due to a thin adherent epiretinal membrane (Figure 2E). In the right eye, the presence of highly reflective vitreous bands superiorly and superotemporally to the macula generating retinal traction were detectable (Figure 2, G and H). The central retinal thickness was markedly reduced in both eyes as a result of retinal atrophy, mainly of the outer retinal layers. The external limiting membrane and the ellipsoid layer were not detectable (Figure 2, E and F).[15]

Full-field ERG revealed a nonrecordable waveform for all cone and rod responses in both eyes. The EOG showed an absent light rise in both eyes (Table 1).

Patient IV: 3, daughter of the proband, a 21-year-old white woman, was first seen by an ophthalmologist at the age of 14. Her visual acuity was 0.2 logMAR (20/32) in both eyes at that time. When we examined her at age 21, her best-corrected visual acuity was 0.4 logMAR (20/50) in both eyes. Her refraction was S + 1.00 = C + 2.25 @ 90° in the right eye and S + 1.75 = C + 2.00 @ 90° in the left eye. Biometric assessment showed an AXL of 20.43 mm with an ACD of 3.06 mm in the right eye, and an AXL of 20.49 mm and ACD 3.09 mm in the left eye. Biomicroscopic examination of the fundus showed cystoid changes in the macula with mild pigmentary irregularities in both eyes, associated with atrophic-appearing round zones in the midperiphery (Figure 3, A and B).

Fundus autofluorescence showed hyperautofluorescence in the macula in both eyes, corresponding to cystoid fluid collections on spectral domain optical coherence tomography (Figure 3, C and D). Similar to her mother (III: 7), a diffuse oval-shaped zone of hyperautofluorescence was seen in the area of the retinal vascular arcades in both eyes (Figure 3, C and D). Horizontal spectral domain optical coherence tomography through the fovea showed intraretinal cystoid fluid collections and subretinal fluid accumulation in both eyes (Figure 3, E and F) and a discontinuous increased reflectivity of the vitreoretinal interface in the left eye (Figure 3F). Full-field ERG revealed a reduced scotopic 0.01 ERG amplitude, reduced scotopic 3.0 ERG amplitude, reduced photopic 3.0 ERG, and photopic 3.0 flicker ERG amplitude with delayed implicit time in both eyes. The EOG light rise was present but was markedly reduced (Arden ratio of 1.17 in the right eye and 1.22 in the left eye) (Table 1).

Patient IV: 2 (son of the proband), a 23-year-old white man, was diagnosed by an ophthalmologist with "macular dystrophy" at the age of 16. At that time, his visual acuity was 0.4 logMAR (20/50) in both eyes. Fluorescein angiography performed at the age of 18

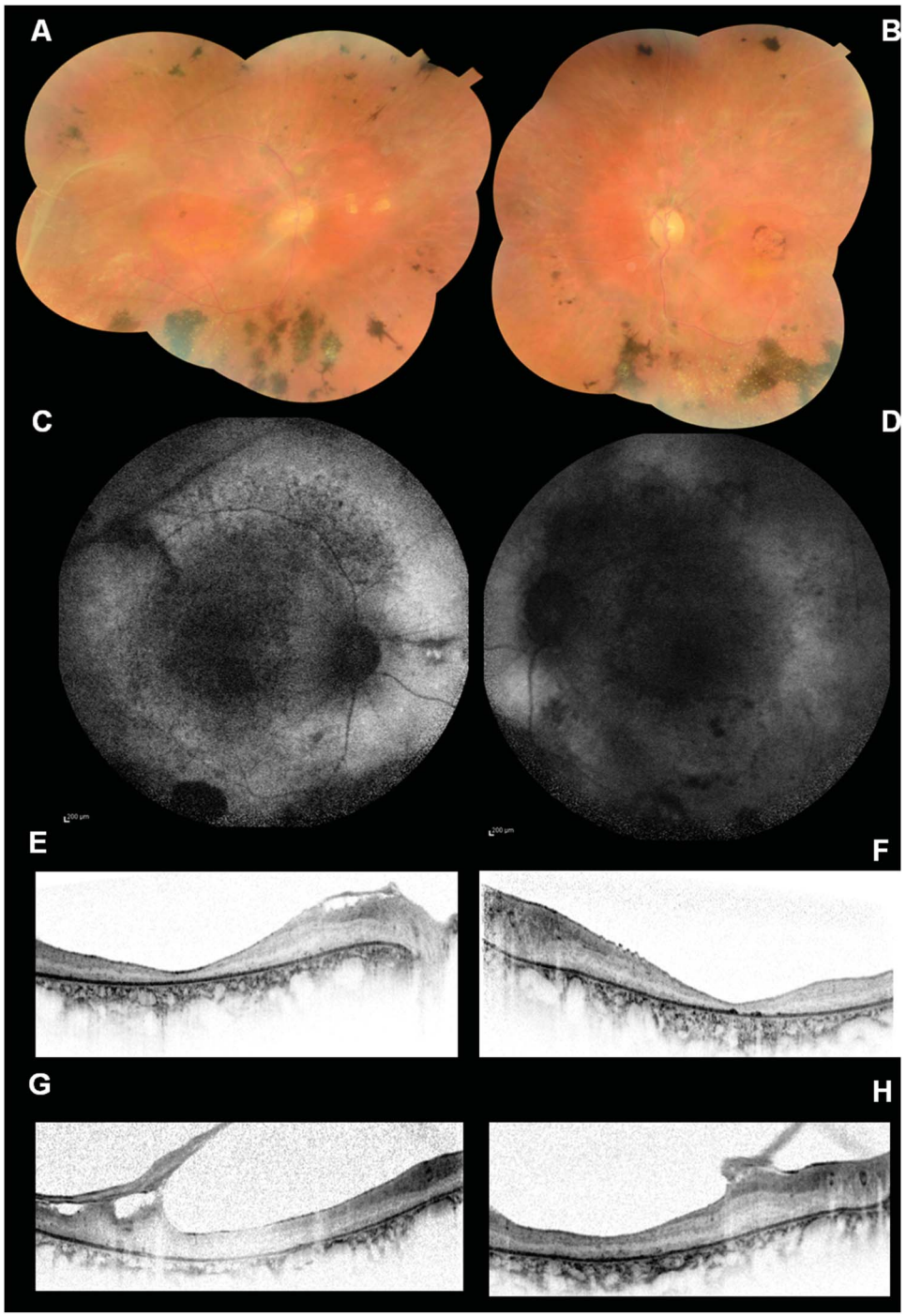

Fig. 2. Images of the 46-year-old proband (III: 7) with a visual acuity of hand movements in both eyes. **A** and **B.** Color fundus photograph of the right and left eye showing vessel attenuation, RPE-choriocapillaris atrophic changes in the macular area, yellowish deposits nasally to the optic disc in the right eye. In the periphery extensive areas of hyperpigmentation and yellowish depositions were visible in the inferior, temporal, and nasal sectors. Note the presence of retinal gliosis and vitreous bands throughout the retina. **C** and **D.** Fundus autofluorescence of right and left eyes showed hypoautofluorescence in the posterior pole due to RPE atrophy and hyperautofluorescent areas corresponding to the yellowish subretinal deposits. In the retinal periphery, extensive areas of hypoautofluorescence corresponded to confluent pigment deposits. **E** and **F.** Spectral domain optical coherence tomography of the right and left eye showing a thin adherent epiretinal membrane at the vitreoretinal interface. Vitreous strands were present nasally and superotemporally to the macula of the right eye. The central retinal thickness was markedly reduced in both eyes. **G** and **H.** Epiretinal membranes were seen in both eyes and vitreous strands in the right eye.

showed a hypofluorescent circular area in the macular region possibly due to lipofuscin deposits. When we examined him at age 23, his best-corrected visual acuity was 1.0 logMAR (20/200) in both eyes, with a refraction of S + 5.00 = C + 1.50 @ 110° in the right eye, and S + 6.00 = C + 1.50 @ 45° in the left eye. Biometric assessment showed an AXL of 20.24 mm and an ACD of 3.01 mm in the right eye and an AXL of 20.19 mm and ACD of 3.00 mm in the left eye. Fundoscopy showed a clinical picture that was virtually identical to that of his sister (IV: 3), with cystoid intraretinal fluid collections in both maculae with mild pigmentary changes. Subretinal yellowish deposits were present in the inferior part of the macula and outside the temporal vascular arcade (Figure 4, A and B). Fundus autofluorescence

Table 1. Clinical and Genetic Characteristics of Family Members III: 7, IV: 3, and IV: 2

Patient	Sex	Age at Onset	VA Refraction	Fundoscopy	Autofluorescence	SD-OCT	ERG/EOG	*BEST1* Mutation
III: 7	Female	46 years	OD hand motion (20/20.000); S + 6.75 = C + 0.50 @ 90°; OS hand motion (20/20,000); S + 4.50 = C + 1.50 @10°	OU: attenuation of the retinal arteries, RPE-choriocapillaris atrophic changes in the macula, areas of coarse hyperpigmentation and small dot-shaped yellowish depositions in midperipheral and peripheral retina, mid/peripheral ERMs and vitreous strands; in OD: nasally to the optic disc 2 areas of subretinal yellowish deposits; (Figure 2, A and B)	OU: patchy hypoautofluorescence in the posterior pole due to RPE atrophy; a diffuse oval-shaped zone of hyperautofluorescence in the area of the retinal vascular arcades; in the midperipheral and peripheral retina extensive areas of hypoautofluorescence; corresponded to confluent atrophic zones with hyperpigmentation on ophthalmoscopy; in OD: 2 hyperautofluorescent areas nasally to the optic disc corresponded to the yellowish subretinal deposits on fundoscopy; (Figure 2, C and D)	OU: hyperreflectivity of the vitreoretinal interface due to ERM; markedly reduced CRT; nondetectable ELM and ellipsoid layer; OD: highly reflective vitreous bands superiorly and superotemporally to the macula; (Figure 2, E and F, G, H)	ERG: nonrecordable waveform for all cone and rod responses; EOG: absent light rise	Heterozygous c.614T>C (p.I205T)
IV: 3	Female	21 years	OD 0.4 logMAR (20/50); S + 1.00 = C + 2.25 @ 90°; OS 0.4 logMAR (20/50); S + 1.75 = C + 2.00 @ 90°	OU: cystoid changes in the macula with mild pigmentary irregularities, atrophic-appearing round zones in the midperipheral retina; (Figure 3, A and B)	OU: hyperautofluorescence in the macula, corresponding to cystoid fluid collections; diffuse oval-shaped zone of hyperautofluorescence in the area of the retinal vascular arcades in both eyes; (Figure 3, C and D)	OD: hyporeflective cystoid lesions in the macula; discontinuous increased reflectivity of the vitreoretinal interface in OS (Figure 3, E and F)	ERG: reduced and delayed waveform for all cone and rod responses; EOG: reduced light rise	Heterozygous c.614T>C (p.I205T)
IV: 2	Male	23 years	OD 1.0 logMAR (20/200); S + 5.00 = C + 1.50 @ 110°; OS 1.0 logMAR (20/200); S + 1.75 = C + 2.00 @ 90°	OU: macular cystoid intraretinal fluid collections with mild pigmentary changes; in OD: subretinal yellowish deposits in the inferior part of the macula, outside the temporal vascular arcade, interface due to a thin adherent ERM was visible in both eyes; (Figure 4, A and B)	OU: petaloid hyperautofluorescence at the posterior pole corresponding to the macular cystoid lesions, a diffuse oval-shaped zone of hyperautofluorescence in the area of the retinal vascular arcades; OD: bright focal hyperfluorescent lesions located inferiorly in the macula, corresponding to subretinal yellowish deposits; (Figure 4, C and D)	OU: intraretinal cystoid fluid collections, subretinal fluid accumulation below the outer retina, some ELM and ellipsoid irregularity and disruption; subretinal hyperreflective deposits corresponding to the yellowish deposits visible on fundoscopy, discontinuous increased reflectivity of the vitreoretinal interface; (Figure 4, E and F)	ERG: reduced and delayed waveform for all cone and rod responses; EOG: absent light rise	Heterozygous c.614T>C (p.I205T)

CRT, central retinal thickness; ELM, external limiting membrane; EOG, electro-oculogramERG, electroretinogram; ERM, epiretinal membrane; OD, right eye; OS, left eye; OU, both eyes; SD-OCT, spectral domain optical coherence tomography; VA, visual acuity.

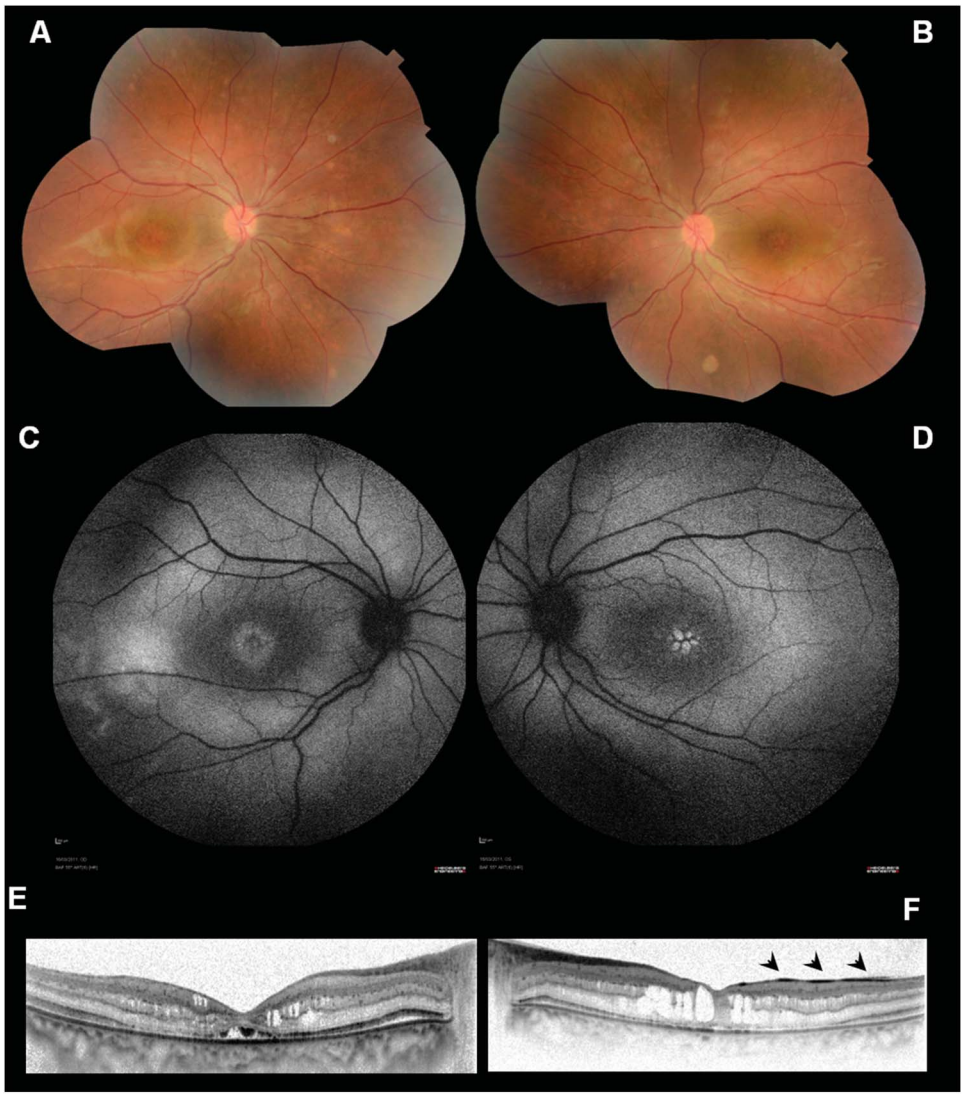

Fig. 3. Images of the 21-year-old daughter of the proband (IV: 3, visual acuity: 0.2 logMAR in both eyes). **A** and **B.** Color fundus photograph of the right and left eye showing cystoid changes in the macular region with mild pigmentary irregularities, associated with yellowish depositions in the nasal sectors of both eyes. **C** and **D.** Fundus autofluorescence of right and left eyes showed hyperautofluorescence in the macula of both eyes, associated with cystoid macular edema in the left eye. **E** and **F.** Spectral domain optical coherence tomography of the right and left eye showing discontinuous increased reflectivity of the vitreoretinal interface in the left eye and intraretinal cystoid changes in both eyes.

showed a petaloid hyperautofluorescence at the posterior pole in both eyes corresponding to the macular cystoid lesions, whereas the right eye also revealed a bright focal hyperfluorescent lesion located inferiorly in the macula corresponding to the subretinal yellowish deposits (Figure 4, C and D). Similar to his mother (III: 7) and sister (IV: 3), a diffuse oval-shaped zone of hyperautofluorescence was seen in the area of the retinal vascular arcades in both eyes. Horizontal spectral domain optical coherence tomography through the macula showed intraretinal large cystoid fluid collections (Figure 4, E and F), and subretinal fluid accumulation with some hyperreflective accumulation below the outer retina in both eyes, with some external limiting membrane and ellipsoid irregularity and disruption (Figure 4, E and F). Subretinal hyperreflective deposits corresponding to the yellowish deposits visible on fundoscopy were visible on optical coherence tomography (Figure 4, G and H). In addition, a discontinuous increased reflectivity of the vitreoretinal interface due to a thin adherent epiretinal membrane was visible in both eyes.

Full-field ERG revealed a reduced scotopic 0.01 ERG amplitude, reduced scotopic 3.0 ERG amplitude, reduced photopic 3.0 ERG, and photopic 3.0 flicker ERG amplitude with a delayed implicit time in both eyes. The EOG showed an absent light peak in both eyes.

Patient III: 9 (sister of the proband), a 42-year-old white woman, was diagnosed by an ophthalmologist with "macular dystrophy" at the age of 13. Fluorescein angiography performed at the age of 23 disclosed patchy hyperfluorescence in the macular region of both eyes due to RPE atrophy with multifocal areas of hypofluorescence. She refused clinical assessment

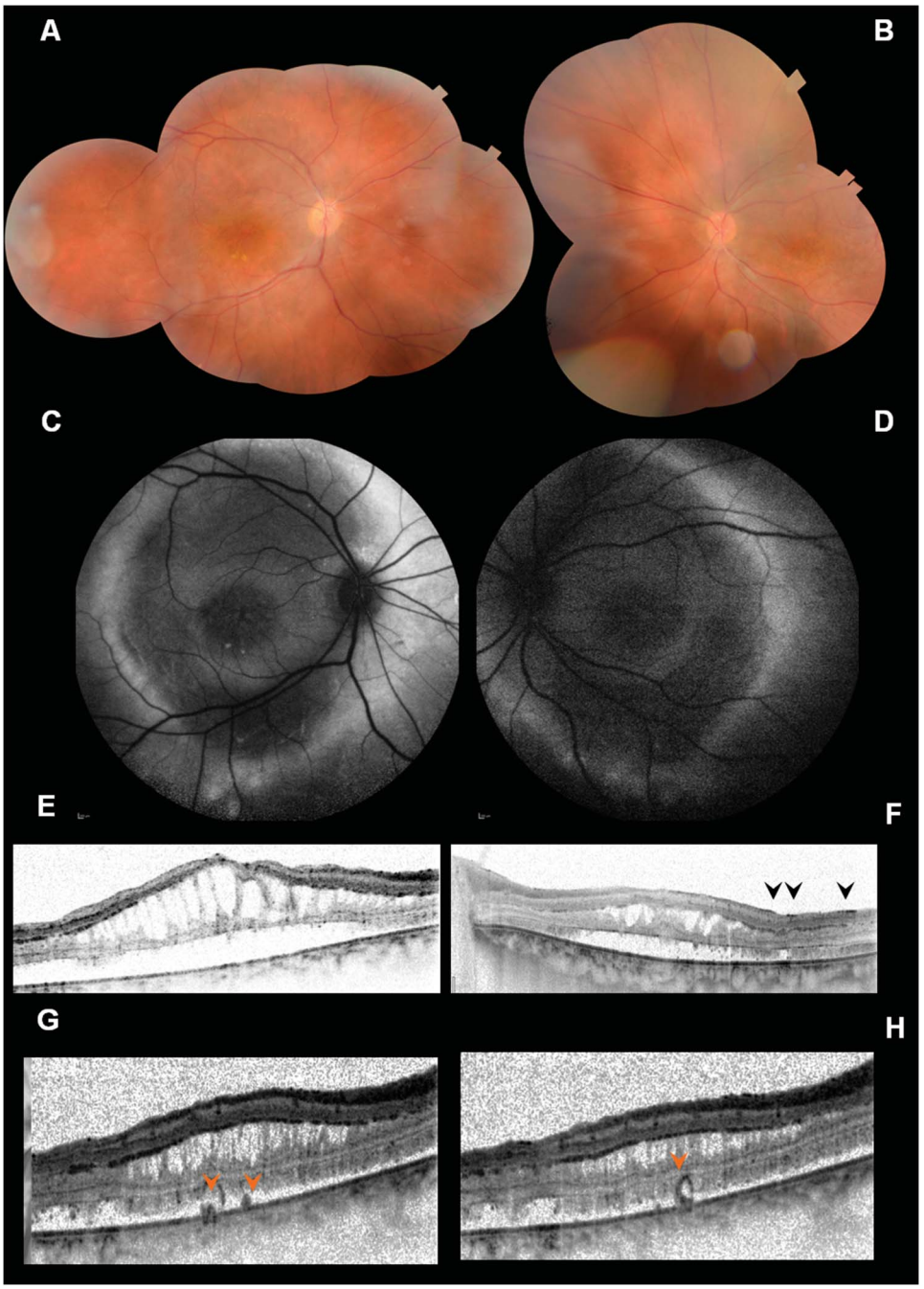

Fig. 4. Images of the 23-year-old son of the proband (IV: 2; visual acuity: 0.4 logMAR in both eyes). **A** and **B.** Color fundus photograph of both eyes showing cystoid changes in the macular region with mild pigmentary changes and subretinal yellowish deposits inferiorly to the macula and externally to the temporal vascular arcade. **C** and **D.** Fundus autofluorescence showing a petaloid hyperautofluorescence in the macula due to the macular edema and a bright focal hyperautofluorescent lesion in the right eye corresponding to the subretinal yellowish deposits. **E** and **F.** Spectral domain optical coherence tomography showing a discontinuous increased reflectivity of the vitreoretinal interface (black arrowheads) and a cystoid macular edema associated with foveo-schisis in both eyes. **G** and **H.** Horizontal spectral domain optical coherence tomography showed some hyperreflective deposits below the neuroretina in both eyes, corresponding to the yellowish deposits visible on fundoscopy (orange arrowhead).

in our department. Patient II: 7 (father of the proband), a 77-year-old white man, was diagnosed by an ophthalmologist with "macular dystrophy" at the age of 40. He refused clinical assessment in our department. Family members I: 2, II: 4, and II: 7 were reported by the proband anamnestically as visually impaired.

Genetic Findings

Genetic analysis showed that all 5 affected members were heterozygous carriers of a c.614T>C (p.I205T) mutation in exon 5 of *BEST1* gene (Figure 5). No other mutations were found in other exons of the *BEST1* gene in any of the affected members.

Discussion

To our knowledge, this is the first report of an autosomal-dominant mode of inheritance in patients diagnosed with a phenotype that strongly resembles or

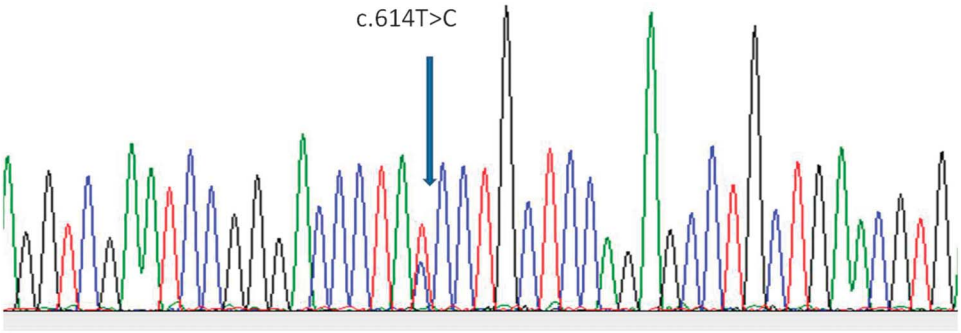

Fig. 5. Sequencing electropherograms showing c.614T>C (p.I205T) in exon 5 of the *BEST1* gene.

is identical to ARB. In contrast to this ARB-like phenotype, the proband of the family showed a striking, severe atypical retinal phenotype showing marked atrophy in the posterior pole, coarse hyperpigmentation in the (mid) peripheral retina, extensive preretinal tractional membranes and vitreous condensations, in combination with a nonrecordable ERG. To the best of our knowledge, this (vitreo) retinal phenotype did not resemble retinitis pigmentosa nor any other phenotype previously described in combination with *BEST1* mutations. In ARB, retinal scarring has been described but not vitreoretinal condensations. These findings in combination with the shallow anterior chamber and short AXL indicate that certain *BEST1* mutations can cause an ocular developmental anomaly phenotype that affects the entire eye.[3,13] Patients IV: 3 and IV: 2 in our study showed a phenotype consistent with previous descriptions of ARB, with yellowish subretinal deposits in the posterior pole (IV: 2), macular cystoid fluid collections, and a neurosensory retinal detachment in the macula associated with reduced ERG flash responses and a markedly reduced or absent EOG light peak.[7,13,19,20]

In a previous study by Davidson et al,[9] the same c.614t>c (p.I205T) variant in *BEST1* was shown to cause an atypical early-onset retinitis pigmentosa-like phenotype, with bilateral total serous retinal detachments associated with epiretinal membrane formation and severe retinal gliosis. Other affected members in the aforementioned family were described as having panretinal dystrophy associated with flecks in the midperipheral retina, retinal gliosis, and severe vascular attenuation, but relatively little peripheral pigment deposition, and an extinguished ERG.[9] This phenotype therefore appears different from the phenotypic range that we describe in this study. Our findings and those of Davidson et al show that the autosomal–dominantly inherited c.614T>C mutation in *BEST1* is associated with a wide spectrum of severe developmental ocular phenotypes, ranging from a phenotype resembling ARB to childhood-onset severe ocular dystrophy, that not only includes vitreoretinal degeneration but also high hyperopia and anterior segment abnormalities.

From the first description of ARB in 2008 by Burgess et al, several authors reported autosomal recessively inherited causal homozygous or compound heterozygous mutations of the *BEST1* gene. The ARB-associated *BEST1* mutations that have reported to date are premature truncations or missense substitutions, and some of them have been hypothesized or demonstrated to cause early transcript degradation or nonfunctional proteins, and are associated with a null phenotype through a markedly decreased or absent bestrophin-1 protein function.[3,10,11,11–14,17,19,20] Previous studies have demonstrated that two ARB missense isoforms severely reduced Cl-channel activity when expressed alone but do not significantly altered the conductance when coexpressed with wild-type bestrophin-1.[3] These results suggested that in these cases carriers with 1 wild-type and 1 mutant allele retain sufficient channel activity to be phenotypically normal, unlike Best disease patients who only require the expression of 1 mutant allele.[3] In contrast, the c.614T>C (p.I205T) *BEST1* variant that we have identified in this study has been tested in human embryonic kidney cell culture, which demonstrated that this mutation produces significantly decreased chloride-selective whole-cell currents in comparison to wild-type protein, even when present in the heterozygous state.[21] This indicates that the heterozygous mutation in the family that we describe is indeed sufficient to cause disease. Given the fact that we did not identify a mutation on the second allele on extensive genetic analysis, in combination with the previous findings by Davidson et al, we believe that autosomal-dominant inheritance of the c.614T>C variant in the *BEST1* gene may be necessary and sufficient to cause this intriguing, severe ocular disease spectrum. However, we were not able to exclude a possible role for deep intronic mutations or modifier genes that may additionally influence the phenotypic outcome, although such genetic influence has not been previously shown.

Possibly, modifier genes in bestrophinopathy can alter the different forms of transmission of disease and phenotypic outcome.[3]

Our study expands the increasingly complex clinical spectrum and heredity of *BEST1*-associated phenotypes, collectively known as the bestrophinopathies.[3] We show that an autosomal-dominant *BEST1* mutation within a single family can not only result in a severe vitreoretinopathy that also affects the entire eye but also in a phenotype that is indistinguishable to that previously described as autosomal recessive bestrophinopathy. In light of these results, a new description may be considered for the variable disease spectrum that may be seen even within a single family. We therefore propose the term "bestrophinopathy", as aspecific as it is. After all, ARB, autosomal-dominant vitreoretinochoroidopathy, MRCS syndrome, and retinitis pigmentosa-like phenotypes are all to a certain degree associated with short AXL and angle-closure glaucoma, as well as panretinal abnormalities on ERG. This clinical spectrum indicates that the entire eye is affected, and functionally and anatomically underdeveloped, albeit to a variable extent that apparently represents a continuum. In contrast to the aforementioned phenotypes, the most common *BEST1*-associated macular phenotypes BVMD and adult-onset foveomacular vitelliform dystrophy are funduscopically and electroretinographically confined to the posterior pole. In addition, BVMD and adult-onset foveomacular vitelliform dystrophy are generally not associated with nanophthalmos, although hyperopia still is more common and angle-closure glaucoma also seems to occur at a higher rate.[22] The pan-ocular abnormalities seen in many *BEST1*-associated phenotypes indicate an additional and important role of the RPE-specific bestrophin-1 protein in ocular development, for instance through interaction with the transcription factors OTX2, MITF, and CRX.[3,23–25]

Our findings may also have implications for future gene therapeutic strategies. Preliminary results of AAV-virus–mediated *BEST1* gene transfer to the RPE in a canine ARB disease model appear promising.[26] However, our findings indicate that autosomal-dominant inheritance in fact underlies some ARB-like phenotypes, which could point to a role for a dominant-negative disease mechanism. More studies would be required to analyze if gene replacement strategies would be sufficient in such cases, or if other or additional strategies are needed such as gene suppression for instance through RNA interference techniques.

Key words: bestrophinopathy, *BEST1* gene, autosomal inheritance.

Acknowledgments

We acknowledge Mariangela Spinogatti for her significant contribution to this study.

References

1. Nordstrom S, Barkman Y. Hereditary macular degeneration (HMD) in 246 cases traced to one gene-source in central Sweden. Hereditas 1977;84:163–176.
2. Petrukhin K, Koisti MJ, Bakall B, et al. Identification of the gene responsible for best macular dystrophy. Nat Genet 1998; 19:241–247.
3. Boon CJ, Klevering BJ, Leroy BP, et al. The spectrum of ocular phenotypes caused by mutations in the BEST1 gene. Prog Retin Eye Res 2009;28:187–205.
4. Gass JD. A clinicopathologic study of a peculiar foveomacular dystrophy. Trans Am Ophthalmol Soc 1974;72:139–156.
5. Patrinely JR, Lewis RA, Font RL. Foveomacular vitelliform dystrophy, adult type. A clinicopathologic study including electron microscopic observations. Ophthalmology 1985;92:1712–1718.
6. Yardley J, Leroy BP, Hart-Holden N, et al. Mutations of VMD2 splicing regulators cause nanophthalmos and autosomal dominant vitreoretinochoroidopathy (ADVIRC). Invest Ophthalmol Vis Sci 2004;45:3683–3689.
7. Burgess R, MacLaren RE, Davidson AE, et al. ADVIRC is caused by distinct mutations in BEST1 that alter premRNA splicing. J Med Genet 2009;46:620–625.
8. Michaelides M, Urquhart J, Holder GE, et al. Evidence of genetic heterogeneity in MRCS (microcornea, rod-cone dystrophy, cataract and posterior staphyloma) syndrome. Am J Ophthalmol 2006;141:418–420.
9. Davidson AE, Millar ID, Urquhart JE, et al. Missense mutations in a retinal pigment epithelium protein, bestrophin-1, cause retinitis pigmentosa. Am J Hum Genet 2009;85:581–592.
10. Burgess R, Millar ID, Leroy BP, et al. Biallelic mutation of BEST1 causes a distinct retinopathy in humans. Am J Hum Genet 2008;82:19–31.
11. Sharon D, Al-Hamdani S, Engelsberg K, et al. Ocular phenotype analysis of a family with biallelic mutations in the BEST1 gene. Am J Ophthalmol 2014;157:697–709.
12. Fung A, Yzer S, Allikmets R. Clinical and genetic misdiagnosis of autosomal recessive bestrophinopathy. JAMA Ophthalmol 2013;131:1651.
13. Boon CJ, van den Born LI, Visser L, et al. Autosomal recessive bestrophinopathy: differential diagnosis and treatment options. Ophthalmology 2013;120:809–820.
14. MacDonald IM, Gudiseva HV, Villanueva A, et al. Phenotype and genotype of patients with autosomal recessive bestrophinopathy. Ophthalmic Genet 2012;33:123–129.
15. Kane Dickson V, Pedi L, Long SB. Structure and insights into the function of a Ca(2+)-activated Cl(-) channel. Nature 2014; 516:213–218.
16. Yang T, Liu Q, Kloss B, et al. Structure and selectivity in bestrophin ion channels. Science 2014;346:355–359.
17. Borman AD, Davidson AE, O'Sullivan J, et al. Childhood-onset autosomal recessive bestrophinopathy. Arch Ophthalmol 2011;129:1088–1093.
18. Crowley C, Paterson R, Lamey T, et al Autosomal recessive bestrophinopathy associated with angle-closure glaucoma. Doc Ophthalmol 2014;129:57–63.
19. Davidson AE, Sergouniotis PI, Burgess-Mullan R, et al. A synonymous codon variant in two patients with autosomal

recessive bestrophinopathy alters in vitro splicing of BEST1. Mol Vis 2010;16:2916–2922.
20. Pomares E, Burés-Jelstrup A, Ruiz-Nogales S, et al. Nonsense-mediated decay as the molecular cause for autosomal recessive bestrophinopathy in two unrelated families. Invest Ophthalmol Vis Sci 2012;53:532–537.
21. Davidson AE, Millar ID, Burgess-Mullan R, et al. Functional characterization of bestrophin-1 missense mutations associated with autosomal recessive bestrophinopathy. Invest Ophthalmol Vis Sci 2011;52:3730–3736.
22. Wittström E, Ponjavic V, Bondeson ML, Andréasson S. Anterior segment abnormalities and angle-closure glaucoma in a family with a mutation in the BEST1 gene and Best vitelliform macular dystrophy. Ophthalmic Genet 2011;32:217–227.
23. Esumi N, Kachi S, Hackler L Jr, et al. BEST1 expression in the retinal pigment epithelium is modulated by OTX family members. Hum Mol Genet 2009;18:128–141.
24. Esumi N, Kachi S, Campochiaro PA, Zack DJ. VMD2 promoter requires two proximal E-box sites for its activity in vivo and is regulated by the MITF-TFE family. J Biol Chem 2007; 282:1838–1850.
25. Esumi N, Oshima Y, Li Y, et al. Analysis of the VMD2 promoter and implication of E-box binding factors in its regulation. J Biol Chem 2004;279:19064–19073.
26. Guziewicz KE, Zangerl B, Komáromy AM, et al. Recombinant AAV-mediated BEST1 transfer to the retinal pigment epithelium: analysis of serotype-dependent retinal effects. PLoS One 2013;8:e75666.